Published in Dalton Transactions, Vol. 45, Issue 4, 2016, p. 1410-1421
which should be used for any reference to this work

NMR spectroscopy and DFT calculations of a self-assembled arene ruthenium rectangle obtained from a combination of coordination and hydrogen bonds†

Divambal Appavoo,[a] Nandhagopal Raja,[a] Robert Deschenaux,[a] Bruno Therrien*[a,b] and Diego Carnevale*[b,c]

The hydrogen-bonded arene ruthenium metalla-rectangle, $[(p\text{-cymene})_2Ru_2(OO\cap OO)(UPy)_2]_2^{4+}$, obtained from 1-(4-oxo-6-undecyl-1,4-dihydropyrimidin-2-yl)-3-(pyridin-4-ylmethyl)urea (UPy) and the dinuclear arene ruthenium clip $(p\text{-cymene})_2Ru_2(OO\cap OO)Cl_2$ (OO∩OO = 2,5-dioxido-1,4-benzoquinonato), is investigated by means of solution-phase NMR spectroscopy. Rotating frame nuclear Overhauser effect measurements are used to probe the H-bond network that drives the UPy self-assembly as well as the full rectangular supramolecular system. An effective distance that takes into account both intra- and intermolecular polarization-transfer pathways is utilised for data analysis. The experimental findings are corroborated by DFT calculations of NMR parameters and internuclear distances, thus confirming the formation of a very stable tetranuclear metalla-assembly.

Introduction

Self-assembly processes involve a small number of simple building blocks that undergo a spontaneous organization into a more complex structure.[1] This is particularly important in supramolecular chemistry, where the possibility of building large systems with desired properties without external intervention or control on the assembly process is extremely appealing. The construction of a superstructure is in fact driven by the interactions taking place between the building blocks themselves. These interactions are usually non-covalent, such as hydrogen bonds, π–π stacking or coordination to metal centres.[2] A careful choice of chemical functionalities aimed at establishing a given intermolecular recognition pattern can allow the engineering of very complex superstructures. This may be conceived and has also been shown in solid-state crystalline systems.[3] The importance of self-assemblies is particularly evident in biological systems. For instance, the folding of proteins in tertiary structures, their subsequent aggregation to form quaternary structures, as well as the formation of the double helical DNA may all be well described as self-assembly processes.

Among the various non-covalent interactions that can be exploited in this context, hydrogen bonding is perhaps the most utilized. Its directionality, stability, reversibility and specificity constitute some of the features that make H-bonding so versatile compared to other non-covalent interactions.[4,5] An appropriate choice of the donor/acceptor pair also allows for tunability of the strength of the H-bonding and hence offers a way of controlling the stability of the resulting self-assemblies. The use of arrays of donor/acceptor pairs can also be considered as a means to regulate the strength of the interactions driving the organization of supramolecular architectures. The latter approach results in parallel arrays of contiguous donor/acceptor pairs on heterocyclic scaffolds capable of establishing a H-bonding network that drives the self-assembly process.[6–11] Examples of up to six consecutive H-bonds have been reported,[12,13] but those involving three and four H-bond arrays are the most studied in molecular recognition and self-assembly of supramolecules.[14–18] Among the most popular scaffolds used to design quadruple H-bonding self-assembled systems is 2-ureido-4-[1*H*]-pyrimidinone (UPy).[19,20] The quadruple H-bonding network of UPy results in the formation of head-to-tail homodimers characterized by high dimerization constants ($k_{dim} > 10^7$ M^{-1}). The use of other complementary non-covalent interactions like metal coordination has recently been reported as a means to synthesize

[a]*Institut de Chimie, Université de Neuchâtel, Avenue de Bellevaux 51, 2000 Neuchâtel, Switzerland*
[b]*Neuchâtel Platform of Analytical Chemistry (NPAC), Institut de Chimie, Université de Neuchâtel, Avenue de Bellevaux 51, 2000 Neuchâtel, Switzerland.*
E-mail: diego.carnevale@unine.ch, bruno.therrien@unine.ch
[c]*Institut des Sciences et Ingénierie Chimiques (ISIC), Ecole Polytechnique Fédérale de Lausanne (EPFL), Avenue Forel 2, 1015 Lausanne, Switzerland*
†Electronic supplementary information (ESI) available. See DOI: 10.1039/c5dt04179a

cyclic superstructures bearing prismatic or cubic cavities, or cages, potentially capable of hosting other molecular species.[21,22] Supramolecular cages assembled by coordination to ruthenium centres have been studied for their applications in anticancer therapy, thanks to their capability to encapsulate, transport and deliver potential drugs to tumour cells.[23,24] Common spacer ligands utilized to form these arene ruthenium assemblies are polydentate pyridyl-based ligands and anionic hydroxybenzoquinonato connectors.[25,26]

A very powerful tool in NMR spectroscopy for structural studies of chemical systems is the Nuclear Overhauser Effect (NOE).[27,28] This technique relies on relaxation phenomena between dipolar coupled spins and manifests itself in changes in signal intensities of nuclear sites when other specific nuclear sites are perturbed by means of a radio-frequency (rf) pulse. More specifically, when the population difference across the Zeeman eigenstates of a nuclear spin is driven away from its equilibrium state, either by saturation or inversion, a change in signal intensity may be observed for resonances associated with spins which are dipolar coupled to the irradiated one. In other words, if a nuclear spin is in spatial proximity to another one, with the latter being perturbed by an rf-pulse, the former will show a variation of signal intensity when compared to a spectrum where no spin is irradiated. A requirement for this phenomenon to take place is a dipolar coupling between the above-mentioned nuclear spins. This interaction is proportional to r^{-6}, where r is the distance between the spin pairs. Therefore, the experimental observation of NOE supplies information about – and implies – spatial proximities between given nuclear sites and can prove to be extremely useful in structural studies of the supramolecular systems considered in this study. It may be shown that, under the conditions of linear growth of the NOE enhancements, if one perturbs the equilibrium–population difference of spin A and observes NOEs on spins B and X, the following relationship applies:[27]

$$r_{AB} = r_A(I_X/I_B)^{1/6}, \quad (1)$$

where I_i is the intensity of the ith signal, and r_{Ai} is the internuclear distance between the irradiated spin A and the ith spin for which the NOE is observed. If the internuclear distance r_{AX} is known, then one can readily determine the unknown distance r_{AB}. A widespread variation of the NOE experiment is the Rotating-frame Overhauser Effect (ROE),[29,30] where an rf pulse is applied so as to spin-lock the magnetization in the transverse plane. This technique is utilized in the cases where NOE enhancements are close to zero. In contrast with the NOE, where the magnetization transfer is related to relaxation along the static B_0 field, in the ROE case relaxation takes place in the transverse field associated with the rf pulse. In spite of these differences, the general discussion about NOE outlined above applies to ROE as well. Therefore, also this latter technique may be utilized for structural studies aiming to determine internuclear distances between sites experiencing non-negligible dipolar couplings.

Density Functional Theory (DFT)[31] calculations of NMR parameters such as chemical shieldings, J couplings or electric field gradients can prove extremely useful in assisting with spectral interpretation and assignment.[32,33] These methods may be utilized in NMR studies aiming at the structural characterization of a variety of chemical systems either in solution or in the solid state.[34–42]

In this context, we turned our attention to the self-assembly of an arene ruthenium rectangle resulting from UPy H-bonded dimers and a hydroxybenzoquinonato arene ruthenium clip. In contrast with previous arene ruthenium assemblies based on classical polydentate pyridyl linkers, these systems consist of a combination of H-bonding and coordination-driven self-assemblies that offer new possibilities in the rational design of cavities with desired functional properties.

We probe the existence of the H-bonding network that characterizes the formation of the UPy homodimer by means of 1D ROESY measurements. The formation of the metalla-rectangle superstructure is also demonstrated using this solution-phase NMR technique. The experimental evidence is corroborated by a computational approach involving semiempirical and DFT calculations. The geometry optimizations of the relevant species supply internuclear distances that can be compared to those determined experimentally by means of NMR ROE measurements whereas the calculations of the magnetic shielding tensors allow for a comparison with the experimental ^{1}H and ^{13}C chemical shifts observed in solution-phase spectra.

Results and discussion

Solution-NMR and computational study of UPy

The hydrogen-bonded arene ruthenium metalla-rectangle, $[(p\text{-cymene})_2Ru_2(OO\cap OO)(UPy)_2]_2^{4+}$, obtained from 1-(4-oxo-6-undecyl-1,4-dihydropyrimidin-2-yl)-3-(pyridin-4-ylmethyl)urea (UPy) and the dinuclear arene ruthenium clip $(p$-cymene$)_2$-$Ru_2(OO\cap OO)Cl_2$ (OO∩OO = 2,5-dioxido-1,4-benzoquinonato), is isolated as its triflate salt. The structure of the arene ruthenium rectangle and the numbering adopted in this study are shown in Fig. 1. Previous attempts aiming at the characterization of such H-bonded systems by means of ^{1}H NMR analysis performed at different concentrations in the mM to μM range did not show any significant variation in chemical shifts thus preventing the determination of the dimerization constant of this highly stable H-bonded self-assembly.[7] The proton spectrum of a solution of UPy in $CDCl_3$ is shown in Fig. 2(a). The assignment of all resonances has been achieved *via* 2D heteronuclear correlation experiments, more specifically HSQC and HMBC (Fig. ESI1 and ESI2,† respectively), and is presented in Table 1. Fig. 2(b)–(d), show 1D ROESY spectra of the same sample where H(2), H(10) and H(13) were irradiated, respectively. When analysing NOE enhancements in such dimeric structures one has to consider both intra- and intermolecular dipolar couplings, which may both supply pathways for polarization transfer. If one

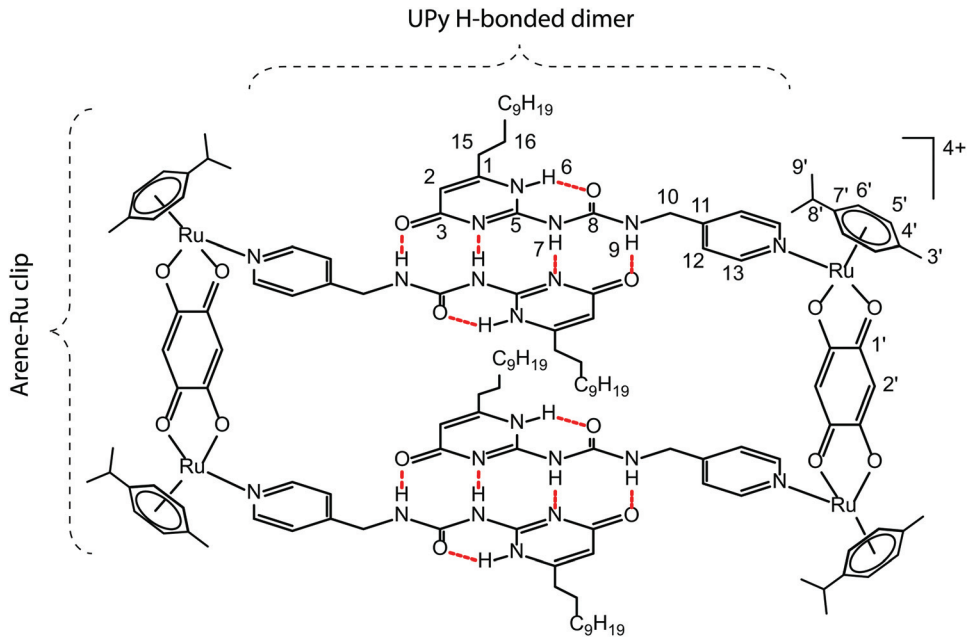

Fig. 1 Molecular structure and numbering scheme for $[(p\text{-cymene})_2Ru_2(OO\cap OO)(UPy)_2]_2^{4+}$.

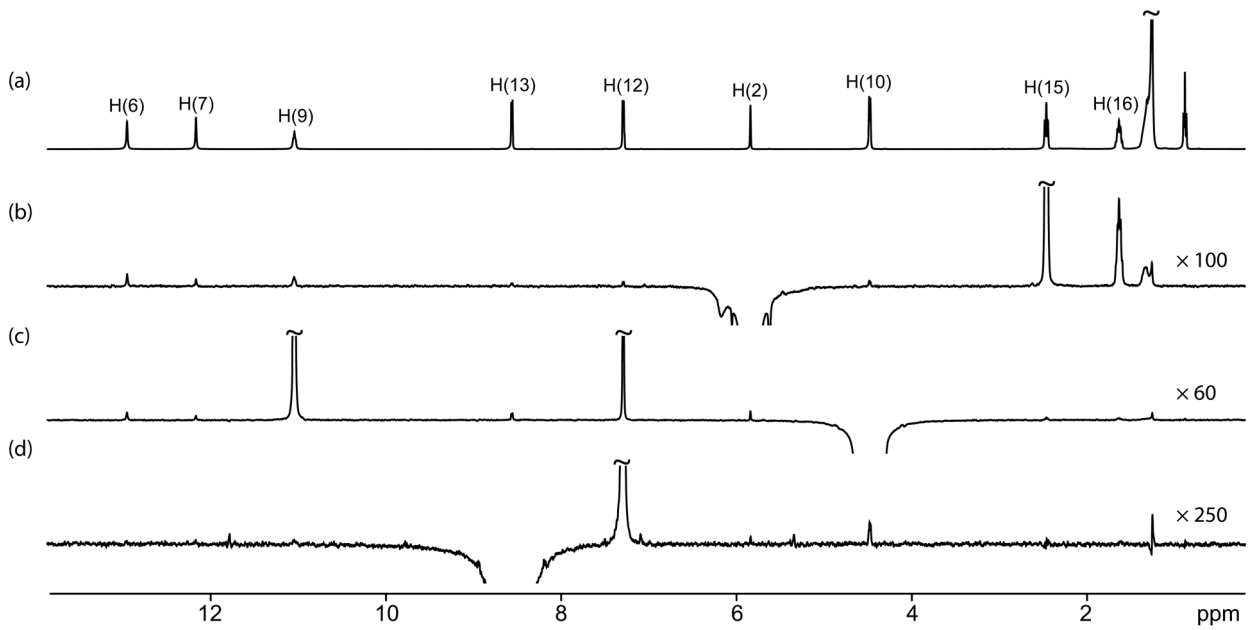

Fig. 2 (a) Proton spectrum of UPy in $CDCl_3$ at 9.4 T with assignment of the relevant peaks. (b)–(d) 1D ROESY spectra of the same sample of (a) with selective irradiation of H(2), H(10) and H(13), respectively.

considers two spins A and B belonging to one molecule and their chemically-equivalent counterparts A′ and B′ belonging to the other molecule of the dimer, it may happen, as in our case, that $r_{AB} > r_{AB'}$. In other words, the NOE enhancement observed for, say, the spin B (and B′) when perturbing the spin A (and A′) may be related to both intra- and intermolecular dipolar couplings. This concept is depicted in the scheme shown in Fig. 3(a), where the head-to-tail homodimer is represented as two triangles and intra- and intermolecular polarization-transfer pathways between two sites A and B are indicated by dashed grey arrows, and labelled as r_{AB} and $r_{AB'}$, respectively. In order to take into account these effects, eqn (1) needs to consider an effective distance $r_i^{(eff)}$ that can be related to the intensity of the enhancement I_i of the ith

Table 1 Assignment of ^{13}C and ^{1}H resonances of the UPy in a $CDCl_3$ solution

^{13}C (ppm)	^{1}H (ppm)	Assignment
173.2	—	3
157.0	—	8
154.5	—	5
152.8	—	1
150.0	8.5	13
147.7	—	11
122.1	7.3	12
106.1	5.8	2
42.5	4.5	10
32.7	2.45	15
31.9–14.1	2.45–0.9	Aliphatic chain
—	13.0	6
—	12.2	7
—	11.0	9

spin which is experiencing n different polarization-transfer pathways:

$$r_i^{(\mathrm{eff})} = \left[\frac{1}{r_{i,1}^6} + \frac{1}{r_{i,2}^6} + \ldots + \frac{1}{r_{i,n}^6} \right)^{-1} \Bigg]^{1/6} = \left(\frac{\prod_j^n r_{i,j}^6}{\sum_j^n r_{i,j}^6} \right)^{1/6}. \qquad (2)$$

It is worth noting that these n considered pathways represent direct polarization transfers and any indirect effect due to spin diffusion is neglected in this context.[43] Fig. 3(b) shows a plot of the effective distance $r^{(\mathrm{eff})}(r_1,1)$ as calculated with eqn (2) for two interatomic distances r_1 and r_2, where $r_2 = 1$ and r_1 is linearly increased up to 2 arbitrary units (a.u.) of distance. If $r_1 \ll r_2$, then $r^{(\mathrm{eff})} \sim r_1$ whereas if $r_1 \gg r_2$, then one has $r^{(\mathrm{eff})} \sim r_2$. In the intermediate case of $r_1 \sim r_2$, $r^{(\mathrm{eff})}$ returns a value that is smaller than both r_1 and r_2. More specifically, in the particular case of two $r_1 = r_2 = 1$ a.u., one has $r^{(\mathrm{eff})}(1,1) = 1/\sqrt{6} \approx 0.89$. When, as in our case, spin pairs can experience intermolecular polarization-transfer pathways which are shorter than or similar to intramolecular ones, eqn (2) necessarily needs to be taken into account in order to interpret experimental NOE enhancements.

The histogram in Fig. 4 shows the differences $\Delta r = |r_{\mathrm{ROE}} - r_{\mathrm{DFT}}|$ between internuclear distances measured from the ROE enhancements of the spectra in Fig. 2(b)–(d), and those obtained from the structures of the monomeric and dimeric UPy as optimized with DFT methods. The smaller those differences the better the agreement between experiments and calculations. In other words, the smaller these differences the more likely the DFT structure to resemble that present in the physical sample. In this histogram, the differences calculated assuming a monomeric UPy structure are shown in white whereas those calculated assuming the head-to-tail dimer are shown in grey. In the former case, only intramolecular dipolar couplings were taken into account whereas in the latter case both intra- and intermolecular pathways of polarization transfer were considered by means of eqn (2). This histogram clearly shows a much better agreement of the experimental

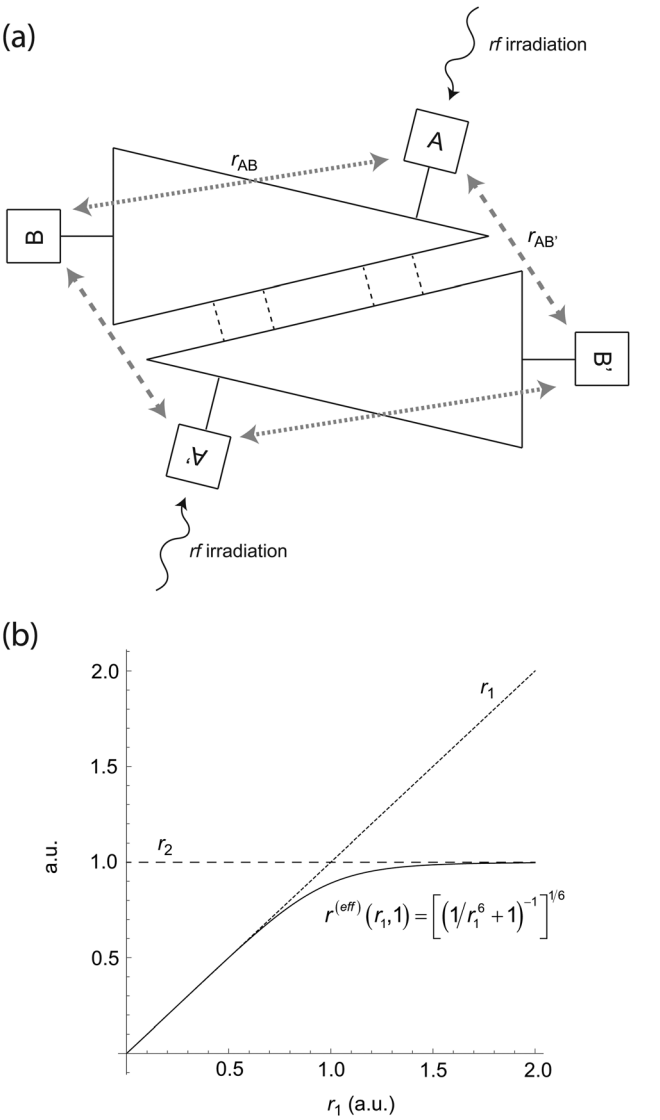

Fig. 3 (a) Schematic representation of the dimeric structure of UPy as a head-to-tail homodimer where the intra- and intermolecular distances between spin pairs involved in NOE/ROE experiments are indicated by thin and thick dashed grey arrows and labelled as r_{AB} and $r_{AB'}$, respectively. For the given arrangement of monomers and location of the sites A and B, intermolecular distances are shorter than intramolecular ones. (b) Plot of the effective distance $r^{(\mathrm{eff})}(r_1,1)$ as calculated using eqn (2) for two interatomic distances r_1 and r_2, where $r_2 = 1$ and r_1 is linearly increased up to 2 arbitrary units (a.u.) of distance.

datasets when the dimeric structure is considered, with differences generally smaller than 1 Å in all cases. In particular, proton sites which are on opposite sides of the structure, such as, say, H(2) and H(13), necessarily require intermolecular pathways which may only exist in the dimer in order to interpret the experimentally-observed ROE enhancements. In the case of a monomeric UPy, in fact, one obtains mismatches as large as 3 Å. It is also interesting to note that the effective multi-pathway distance $r_1^{(\mathrm{eff})}$ reproduces roughly the same results as the monomeric single-pathway one for those protons

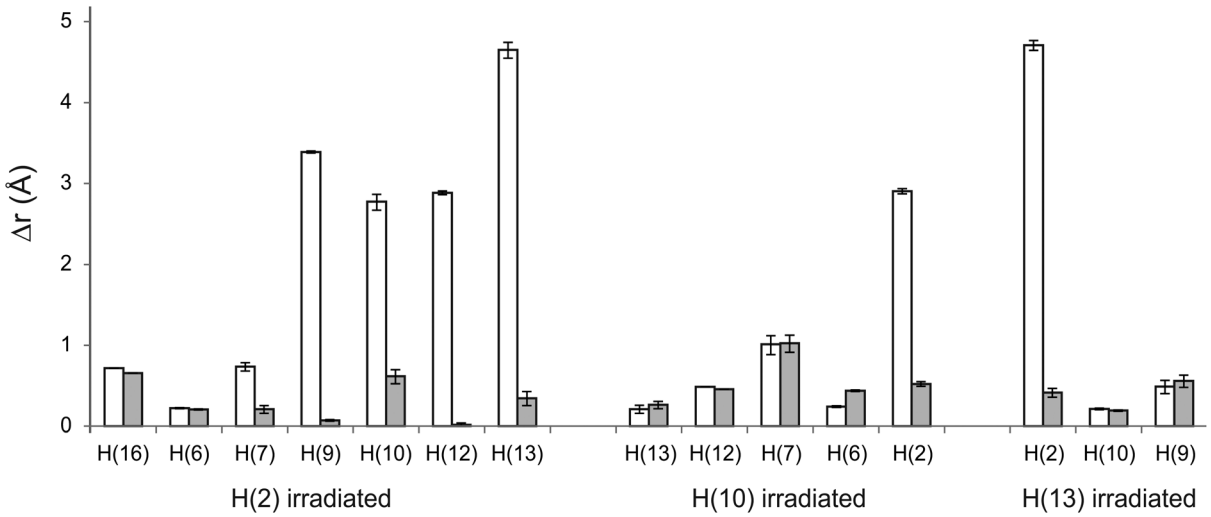

Fig. 4 Histogram of the differences $\Delta r = |r_{ROE} - r_{DFT}|$ between distances as measured by ROE experiments and those calculated with DFT methods. Data represented by white rectangles refer to a monomeric structure whereas grey ones refer to a H-bonded dimer of UPy. The error bars refer to the experimental data and were calculated using eqn (1) and (2) where the intensity of enhancement of the *i*th spin was $I_i = \overline{I} \pm \sigma_i$, with $\overline{I}_i$ being the average intensity of four independent integrations of the *i*th peak and σ_i being the standard deviation of four integral values. Numerical values are given in Tables ESI1 and ESI2.†

located in the central part of the structure. It is worth noting that the enhancement obtained on H(13) when H(2) is irradiated is very consistent with that obtained on H(2) when H(13) is irradiated. The same consistency is obtained also for the other couple of sites H(2) and H(10).

The experimental data based on 1D ROESY measurements presented so far strongly indicate the existence of UPy as a H-bonded dimer in solution. An independent further assessment was also carried out by considering the chemical shifts of the ^{13}C and ^{1}H resonances as measured in conventional 1D spectra and those calculated by DFT methods.

Fig. 5(a) shows the correlation between experimental ^{13}C chemical shifts and those calculated for the monomeric structure. The quality of the correlation may be indicated by a coefficient $R^2 = 0.996$. Fig. 5(b) shows the analogous correlation when the dimeric structure was used to calculate the chemical shifts. In this latter case $R^2 = 0.999$, with all carbon sites very accurately described by the DFT calculations and lying very close to the ideal 1 : 1 correlation represented by the dashed line. Fig. 5(c) shows the correlation between experimental ^{1}H chemical shifts and those calculated for the monomeric structure. In this case, the NH protons lie completely out of the ideal correlation line where all other proton sites are instead found. These protons are involved in the H-bonding network that assembles the dimeric structure. If solvent effects are included in the calculations, no substantial improvement is obtained, as indicated by the empty dots. Fig. 5(d) shows the analogous correlation when the dimeric structure was considered in the calculations. In this case the chemical shifts of the NH protons correlate very well with the calculated ones, with an overall coefficient $R^2 = 0.998$. These results indicate that, in order to interpret the chemical shifts observed experimentally for both ^{13}C and ^{1}H of UPy, a dimeric arrangement needs to be considered. This is particularly true for the protons of the NH groups involved in the H-bonding system.

All the NMR data experimentally observed as ROE ^{1}H enhancements and ^{1}H and ^{13}C chemical shifts strongly support the hypothesis of UPy existing as a head-to-tail homodimer in the solution phase.

Solution-NMR and computational study of the rectangular self-assembly

Subsequently, we turned our attention to the full rectangular complex. The corresponding proton spectrum acquired in a $CDCl_3$ solution is shown in Fig. 6(a). The full assignment of ^{1}H and ^{13}C resonances has been carried out using HSQC and HMBC spectra (Fig. ESI3 and ESI4,† respectively) and is reported in Table 2. The spectral region relevant in our study has been expanded in the inset. When compared to that of Fig. 2(a), one finds considerably broader signals, indicating that a larger species is present in solution. This finding is already indicative of the formation of a larger supramolecular complex. One other feature which is worth noting are the shoulders present in some peaks like, say, H(13). Other sites such as H(12) are represented in the spectrum as a series of partially-overlapped peaks.

These observations indicate a degree of inhomogeneity in the sample. In fact, upon coordination to the ruthenium centre, the chemical equivalence of sites such as, say, the two H(13), is lifted. This necessarily results in different environments for all chemical sites and justifies the above-mentioned inhomogeneous features observed in the spectrum of Fig. 6(a).

In contrast with UPy and its H-bonded dimer where the observation of NOE/ROE effects had to be analysed

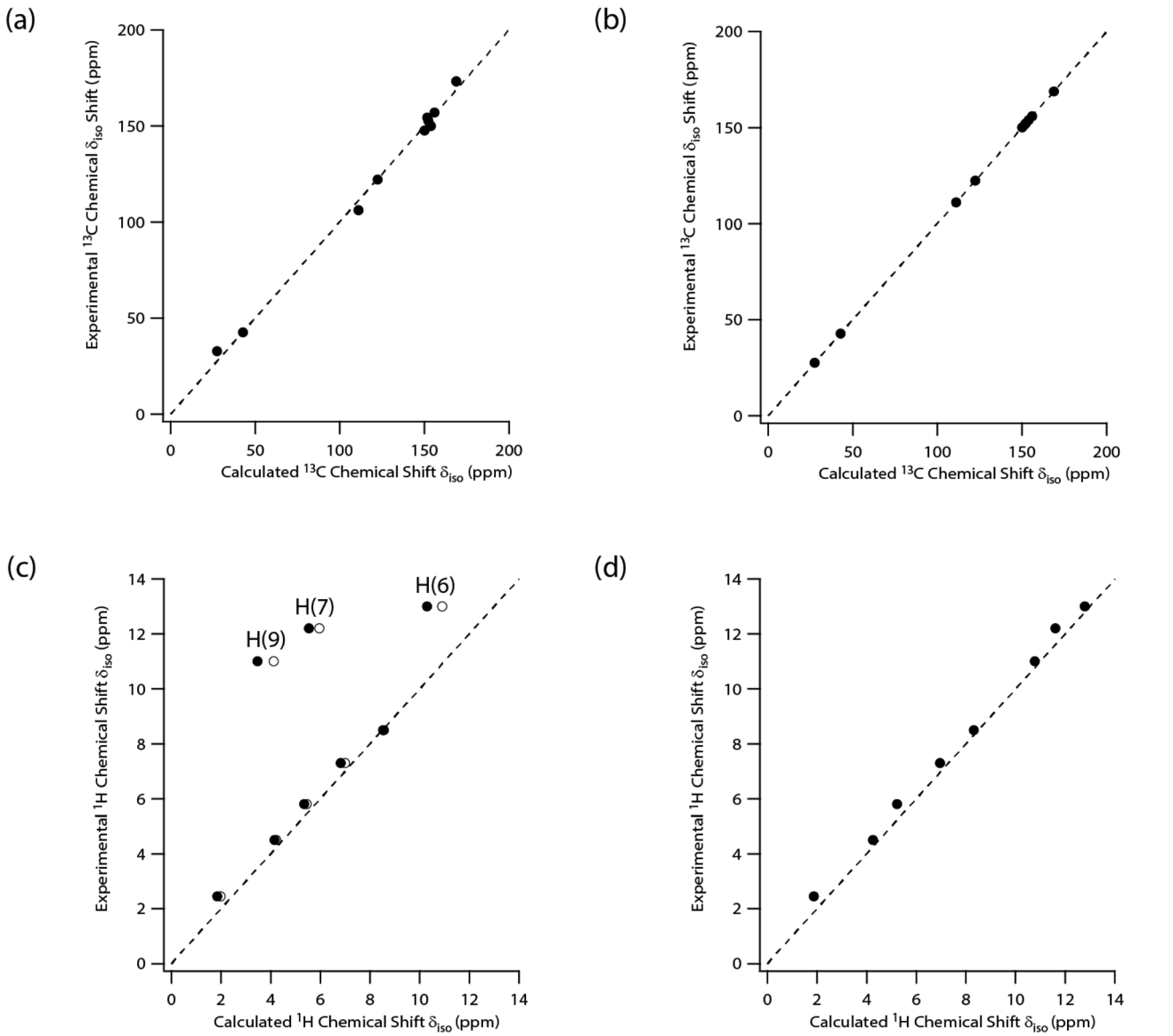

Fig. 5 (a) Correlation between the experimental ^{13}C chemical shifts of a UPy in a $CDCl_3$ solution and those calculated using DFT methods for UPy. (b) Correlation between the same experimental ^{13}C chemical shifts of (a) and those calculated using DFT methods for the H-bonded dimer. (c) Correlation between the experimental ^{1}H chemical shifts of UPy in a $CDCl_3$ solution and those calculated using DFT methods. The white and black dots refer to calculations where the solvent was, and was not, included, respectively. (d) Correlation between the same experimental ^{1}H chemical shifts of (c) and those calculated using DFT methods on a dimeric structure of UPy. The dashed lines indicate the ideal 1 : 1 correlation in all cases. Numerical values are given in Table ESI3.†

quantitatively to look for evidence of the existence of the dimer (in fact, a polarization transfer between two proton sites may exist in both its monomeric and dimeric structures, it is only the intensity of such transfer that can be related to one of the two hypotheses), NOE/ROE experiments performed on the full complex can provide direct evidence of the formation of the supramolecular system in the solution phase. If fact, a polarization transfer between protons belonging to UPy and protons belonging to the arene ruthenium clip could only be possible if the full structure had undergone self-assembly and would therefore indicate the presence of the rectangular complex in solution. An optimal proton site for the search of intermolecular NOE/ROE is represented by H(13), which is expected to be in the proximity of the bridging benzoquinone once the tetranuclear complex is formed. Fortunately, the peaks associated with this environment (at *ca.* 8.2 ppm) are not overlapped with other sites in the 1D ^{1}H spectrum and can be selectively irradiated in a ROE experiment. Fig. 6(b) shows the corresponding spectrum. Besides the nearby H(12) site, one can clearly see enhancements for the proton sites of the arene Ru clip H(2′), H(5′) and H(6′). This finding clearly indicates that the UPy has coordinated the ruthenium center and

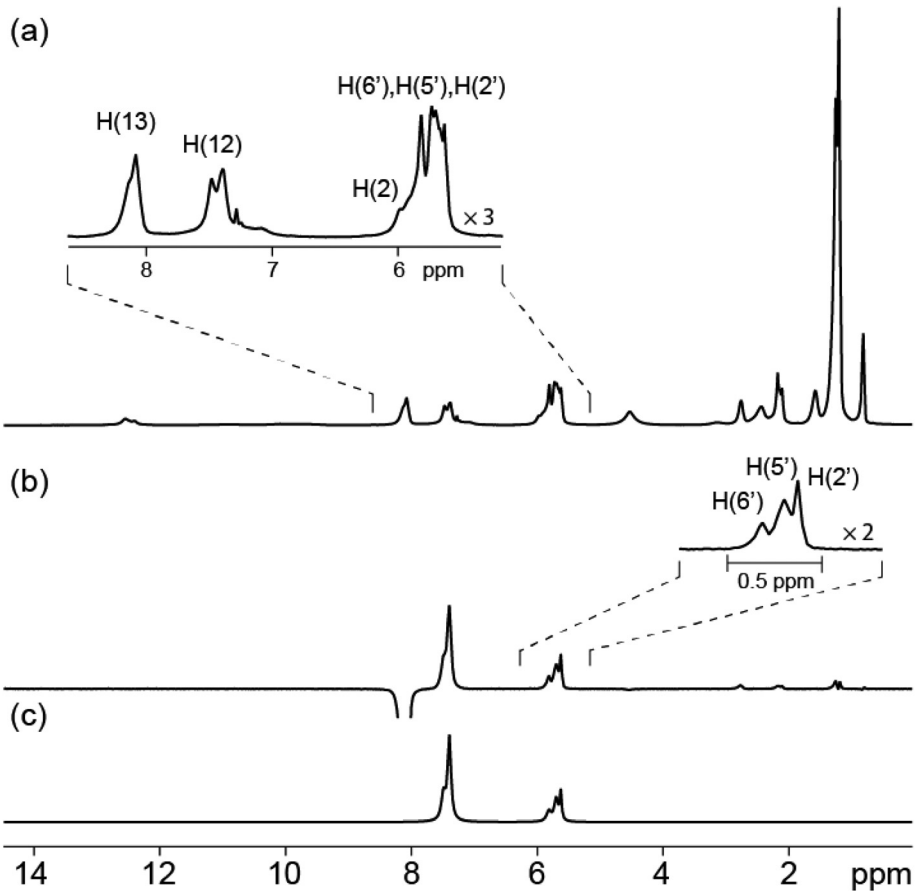

Fig. 6 (a) ^{1}H NMR spectrum of $[(p\text{-cymene})_2Ru_2(OO\cap OO)(UPy)_2]_2^{4+}$ in $CDCl_3$. The relevant peaks involved in our ROE experiment are shown expanded in the inset. (b) 1D ROESY spectrum performed on the same sample of (a) with selective irradiation of H(13). The inset shows an expansion of the resulting ROE enhancements. (c) Numerical fit of the ROE enhancements of (b) assuming five Lorentzian lineshapes, of which two were used for the H(12) peak and the other three for H(6′), H(5′) and H(2′). The resulting intensities of the individual lineshapes were used as a measure of ROE enhancement.

is experimental proof of the formation of the self-assembly. The corresponding spectral region is expanded in the inset. These three environments are better resolved when compared to their appearance in the inset of Fig. 6(a). The ROE experiment in fact acts as a filter allowing the detection of only sites which are dipolar-coupled to the irradiated one and, in turn, yields a spectrum with resonances belonging to the full complex only, filtering out signals associated with unbound species. Fig. 6(c) shows a numerical fit of the ROE enhancements of (b), assuming isotropic Lorentzian lineshapes. Two of these lineshapes have been assumed for the fit of the H(12) resonance in order to account for the shoulder appearing on this peak. The intensities of the single components of this fit can be used as a measure of the experimental ROE enhancements and can be related to internuclear distances as calculated using computational methods. Fig. 7 shows a histogram of the differences $\Delta r = |r_{ROE} - r_{DFT}|$ between the internuclear distances measured from the ROE enhancements of the spectrum in Fig. 6(b), and those obtained from the structures optimized using DFT methods. The white, light grey and dark grey rectangles refer to three rectangular structures produced by

Table 2 Assignment of ^{13}C and ^{1}H resonances of the rectangular self-assembly in a $CDCl_3$ solution

^{13}C (ppm)	^{1}H (ppm)	Assignment
184.0	—	1′
170.9	—	3
155.7	—	8
155.5	—	5
153.4	—	1
152.2	8.11	13
152.0	—	11
124.9	7.43	12
105.7	5.90	2
103.5	—	7′
102.1	5.68	2′
98.7	—	4′
83.3	5.84	6′
82.6	5.72	5′
42.4	4.56	10
33.0	2.47	15
31.7	2.81	8′
22.7	1.31	9′
18.1	2.22	3′
31.9–14.1	2.45–0.9	Aliphatic chain
—	10.95	6
—	10.30	7
—	9.93	9

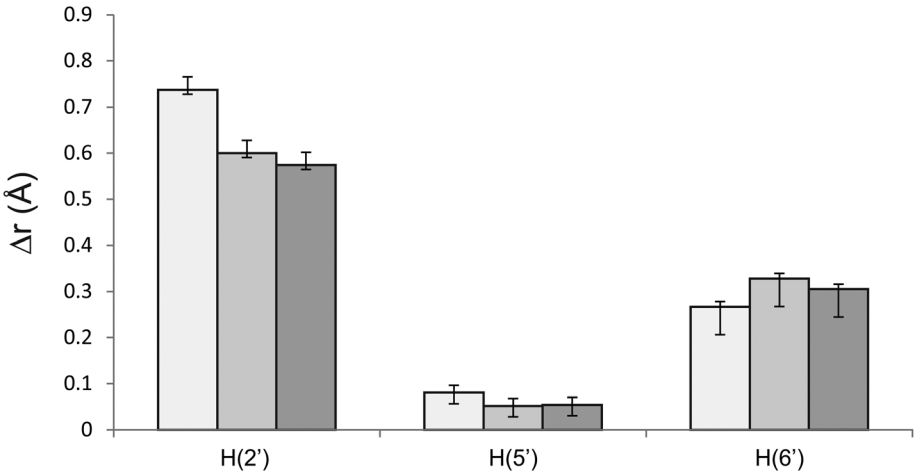

Fig. 7 Histogram of the $\Delta r = |r_{ROE} - r_{DFT}|$ differences between the internuclear distances as measured from the experimental spectrum of Fig. 6(b) and those calculated using DFT methods for $[(p\text{-cymene})_2Ru_2(OO\cap OO)(UPy)_2]_2^{4+}$. White and light grey data refer to structures where the preliminary semiempirical optimization using the PM7 method was performed without, and with, the keywords LET and DDMIN = 0.0, respectively, as implemented in MOPAC2012. Dark grey data refer to a structure where four chloride counterions were added in the proximity of the *p*-cymene rings. Numerical values are given in Tables ESI4 and ESI5.†

the preliminary geometry optimization performed at the semiempirical level with MOPAC2012.[44] These three structures are shown in Fig. 8(a)–(c), respectively. In the case of Fig. 8(a), a wide cavity can clearly be seen. The structure in Fig. 8(b) was produced by a further semiempirical optimization step of that of Fig. 8(a) by means of the keywords LET and DDMIN = 0.0, and results in a partial shrinking of the cavity. In the structure in Fig. 8(c), four chloride counterions were included in the proximity of the *p*-cymene moieties. A further shrinking of the cavity is produced in the latter case. The histogram of Fig. 7 indicates that these three structures produce similar differences with the experimental measurements, with Δr generally always smaller than 1 Å. Fig. 8(d) shows the top view of the structures of Fig. 8(a) where one can appreciate the integrity of the H-bonding network holding together the UPy dimeric moieties of the complex. It is worth mentioning that, in spite of a progressive distortion of the H-bonding system induced by the shrinking of the cavity in the structures of Fig. 8(b) and (c), all the H-bond interactions are preserved also in these two cases. Furthermore, in the case of Fig. 8(c), where counterions are included in the geometry optimization, an 'out-of-plane' twisting of the molecular rectangle is also observed.

Fig. 8(e)–(g) illustrate an expansion of one of the corners of the supramolecular rectangles of Fig. 8(a)–(c), respectively. In all the cases, the orange arrows represent the interatomic effective distances $r_i^{(eff)}$ as calculated using DFT methods, whereas the red ones represent those measured experimentally with ROE spectra. The differences in length between these orange and red arrows are proportional to the values reported in the histogram of Fig. 7. Fig. 8(e)–(g) offer a visual estimation of the good accuracy of our study. Generally, our ROE measurements on the rectangle return slightly shorter internuclear distances when compared to our computational models. However, these mismatches are always smaller than 0.74, 0.60 and 0.59 Å, for the structures of Fig. 8(a)–(c), respectively.

The convergence criteria for the optimizations performed at the higher level of theory for the full complexes were set to a variation of energy smaller than 5×10^{-1} kJ mol^{-1} whereas for the UPy in both its monomeric and dimeric structures the variation of energy was smaller than 2×10^{-3} kJ mol^{-1}. Given these differences in convergence criteria, evaluations of the variations of energy associated with the formation of the H-bonded dimer and the rectangle may not be considered at the DFT level. Nonetheless, full convergence in the geometry optimizations was achieved for all the considered species at the semiempirical PM7 level. When considering the heats of formation at $T = 298$ K as calculated by MOPAC2012,[44] we find that the formation of a H-bonded dimer from two isolated UPy molecules results in a gain of energy $\Delta E = -218.1$ kJ mol^{-1} (-52.1 kcal mol^{-1}). The formation of a supramolecular rectangle from two H-bonded UPy dimers and two arene ruthenium clips results in a variation of energy $\Delta E = -146.8$ kJ mol^{-1} (-35.1 kcal mol^{-1}). This is in agreement with the high stability observed for tetranuclear arene ruthenium complexes.[45]

The possibility of one single UPy H-bonded dimer coordinating one single arene-Ru clip has also been considered at the semiempirical/PM7 level. Two structures have been optimized in this context and are shown in Fig. ESI5 and ESI6.† The corresponding Cartesian coordinate *xyz* files are also given in the ESI.†

It is known that the B3LYP hybrid functional is characterised by a poor description of London dispersion forces and/or dipole–dipole interactions.[46] Therefore, the M06 hybrid functional,[47,48] *ad hoc* parametrised so as to take into account those non-covalent contributions, has also been considered in

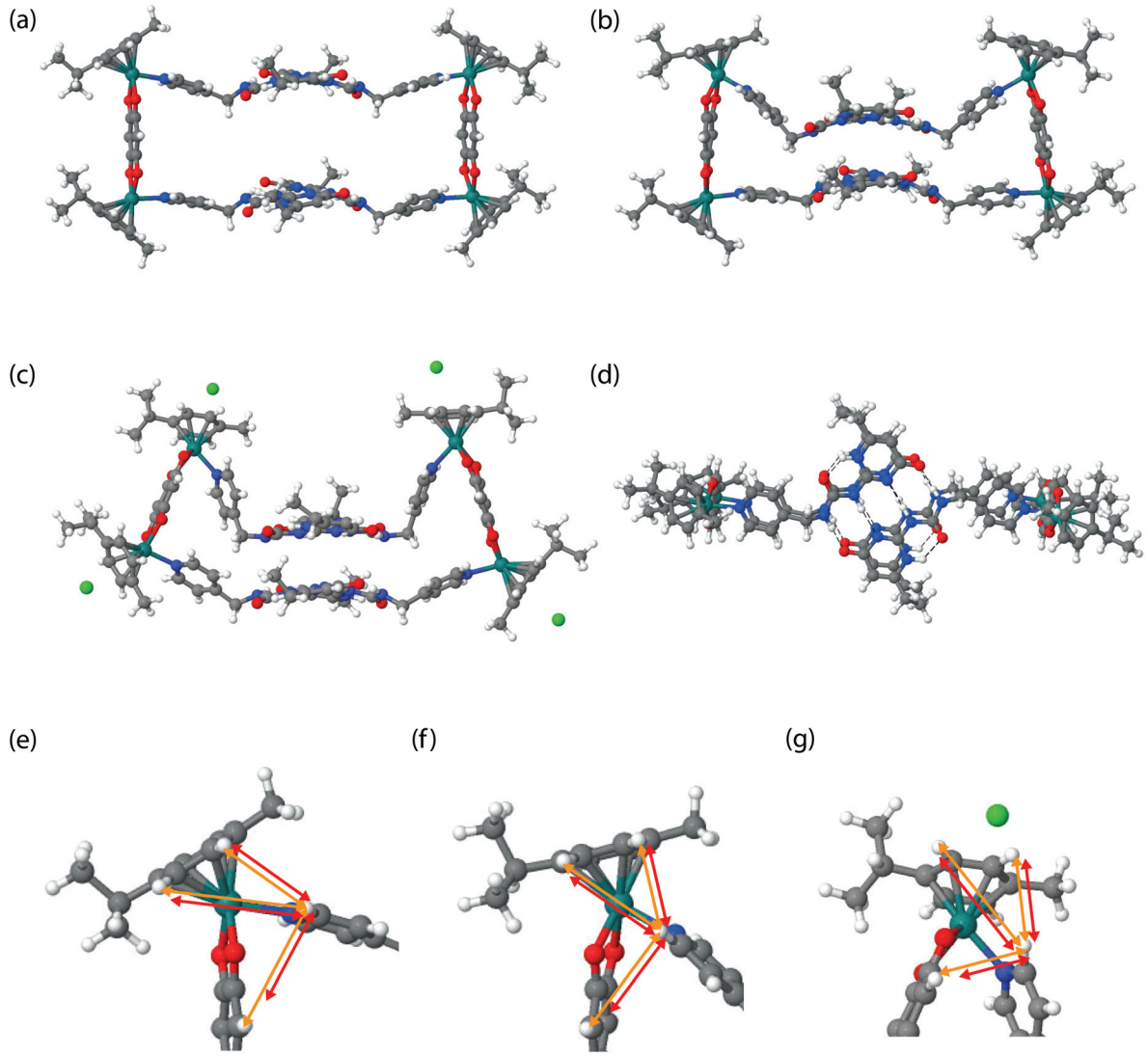

Fig. 8 (a) Structure of $[(p\text{-cymene})_2Ru_2(OO\cap OO)(UPy)_2]_2^{4+}$ as optimized using DFT methods. (b) The same structure of (a) where the preliminary semiempirical optimization step was allowed to proceed further resulting in a shrunk cavity. (c) Structure where four chloride counterions were included and optimized as in (b). (d) Top view of the structure of (a) where one can see the integrity of the H-bonding network. The aliphatic chains of UPy were truncated to ethyls to reduce the computational time. (e) Expansion of the top-left corner of (a). The orange arrows represent the interatomic distances as produced by the calculations whereas the red ones represent the same distances as experimentally measured in our ROE experiments. (f) Expansion analogous to (e) of the structure in (b). (g) Expansion analogous to (e) of the structure in (c). In (e)–(g), the differences in the length between orange and red arrows represent the data shown in Fig. 7 as white, light grey and dark grey rectangles, respectively. H, C, O, N, Cl and Ru atoms are shown in light grey, dark grey, red, blue, green and light blue, respectively. Cartesian coordinate *xyz* files are given in the ESI.†

our study with the 6-31+G(d,p) basis set. The corresponding rectangular structure is shown in Fig. ESI7.† No substantial differences with the B3LYP-optimised structures shown in Fig. 8 are observed in terms of interatomic distances relevant to our ROE measurements. The corresponding Cartesian coordinate *xyz* file is given in the ESI.†

Conclusions

The self-assembly of ureido-pyrimidinone to form quadruple H-bonded dimers has been investigated by means of rotating-frame Overhauser effect NMR measurements and DFT calculations. The ROE enhancements are consistent with those resulting from a head-to-tail homodimeric structure, in which intermolecular interatomic distances may be shorter than intramolecular ones. An effective distance $r_i^{(eff)}$ that takes into account all possible polarization-transfer pathways is utilized for data analysis. The DFT calculations of proton and carbon chemical shifts also support the formation of the dimer. ROE measurements also prove the formation of the supramolecular self-assembled rectangle, with polarization transfers observed between the pyridine protons of the H-bonded moiety and those of the arene ruthenium clip.

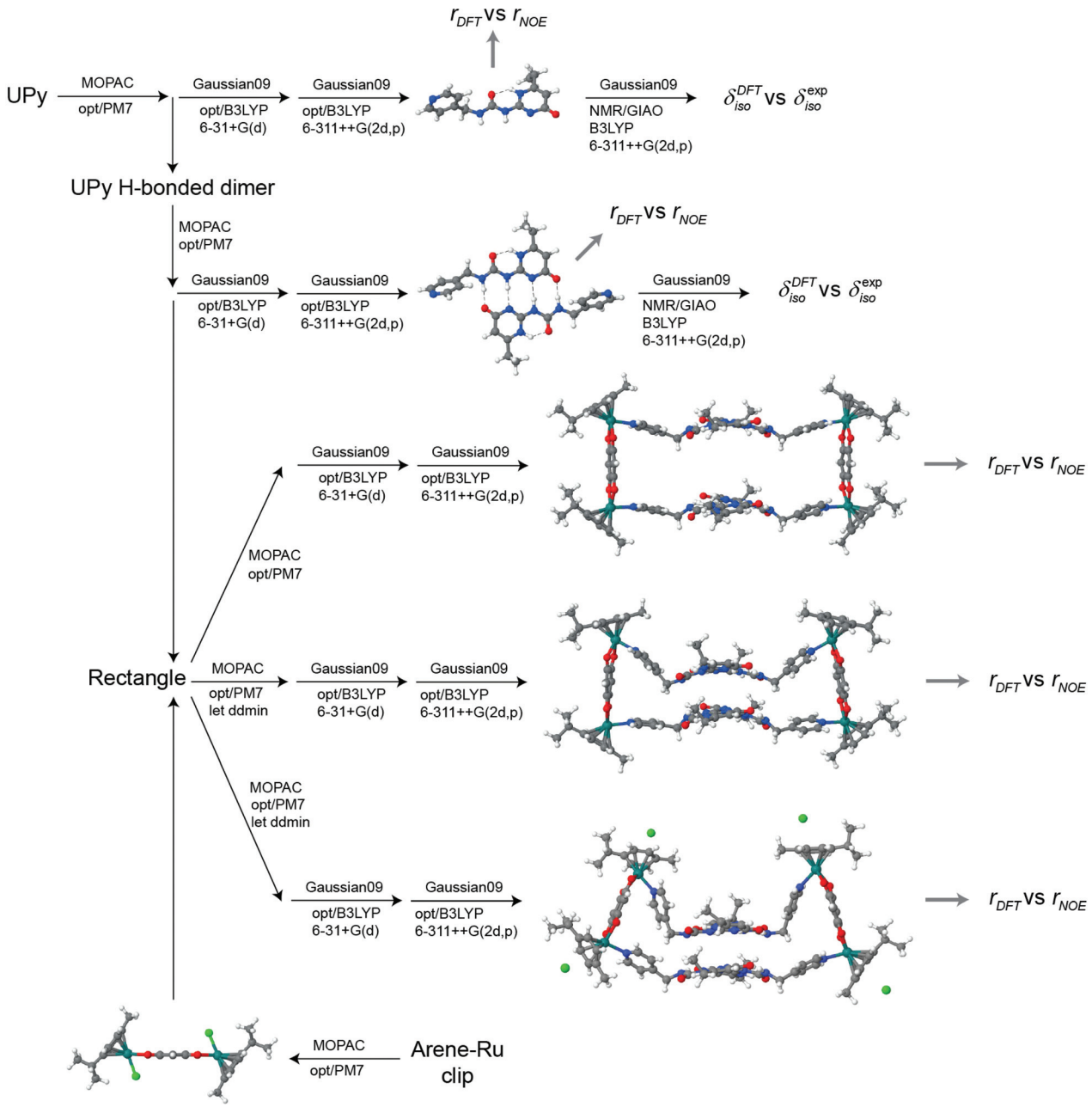

Fig. 9 Representation of the computational scheme adopted in this study. The final structures produced were used for the measurements of internuclear distances to be compared with those measured experimentally with ROE spectra. In the cases of UPy monomeric and dimeric structures, also calculations of ^{1}H and ^{13}C chemical shifts to be compared with those observed experimentally were performed. In order to reduce the computational time, the aliphatic chains of UPy were truncated to ethyls and triflate anions replaced with chlorides.

Experimental section

Solution NMR

All ^{1}H and ^{13}C NMR spectra were acquired on a narrow-bore Bruker 400 spectrometer (9.4 T, $\omega_0/2\pi$ = 400.0 and 100.6 MHz for ^{1}H and ^{13}C, respectively) equipped with an AVANCE-II console and a 5 mm double-resonance probe. The rf-field strengths of all hard $\pi/2$ and π pulses were $\omega_1/2\pi$ = 26 kHz and 27 kHz, for the proton and carbon channels, respectively. The 1D ROESY spectra in Fig. 2 and 6 utilized spin locking with an rf-field strength of 3 kHz and lengths of 150 and 200 ms, respectively, and sinc-shaped selective π pulses of length τ_p = 10 ms.

Computational study

The structures of UPy in both its monomeric and dimeric forms were preliminarily optimized with the semiempirical method PM7 as implemented in MOPAC2012.[44] The same procedure

was also performed on the arene-Ru clip and the full rectangular complex. In the latter case, the optimization was repeated with inclusion of the keywords LET and DDMIN = 0.0, and with four chloride counterions located in the proximity of the *p*-cymene rings. A further optimization was performed with DFT methods utilizing the B3LYP hybrid functional[49,50] and progressively increasing the basis set size from 6-31+G(d) to 6-311++G(2d,p), as implemented in Gaussian09 Revision A.01.[51] The effective-core potentials LANL2DZ[52–54] were used on the ruthenium centres for all DFT calculations. When taken into account, solvent effects were included with the PCM method.[55] The convergence criteria for the DFT optimizations performed at the higher level of theory for the full complexes required variations of energy between two successive geometries to be smaller than 5×10^{-1} kJ mol^{-1} whereas for the UPy in both its monomeric and dimeric structures the variation of energy was smaller than 2×10^{-3} kJ mol^{-1}. The structures thus obtained were used to calculate the magnetic shielding tensors of both ^{1}H and ^{13}C nuclei with the GIAO method[56,57] at the highest level of theory considered for the DFT optimizations. All chemical shifts were referenced to those of TMS at the corresponding level of theory. Fig. 9 shows a scheme representing the overall computational procedure utilized in this work. In order to reduce the computational time required for the DFT steps of the scheme, the aliphatic chains of UPy were truncated to ethyls. The calculations were performed at the EPFL on an Ubuntu Linux 12.04 platform equipped with 16 2.27 GHz CPUs and 24 GB of RAM.

Synthesis

1-(4-Oxo-6-undecyl-1,4-dihydropyrimidin-2-yl)-3-(pyridin-4-ylmethyl)urea (UPy) and the arene ruthenium clip were prepared following literature procedures.[20,23] A mixture of 1 equivalent of $(p\text{-cymene})_2Ru_2(OO\cap OO)Cl_2$ (0.04 g, 0.06 mmol) and 3 equivalents of $AgCF_3SO_3$ (0.04 g, 0.18 mmol) in CH_2Cl_2 (4 mL) was stirred at room temperature for 2 h and filtered to remove AgCl. Then UPy (0.04 g, 0.06 mmol) was added to the filtrate and the solution was stirred at room temperature overnight. The volume of the solvent was halved and diethyl ether was added to precipitate $[(p\text{-cymene})_2Ru_2(OO\cap OO)(UPy)_2]_2(CF_3SO_3)_4$, which was collected as a dark red solid by filtration. A yield of 72% (0.12 g) was obtained. The formation of the tetranuclear arrangement of the full complex was also confirmed by ESI-MS with assignment of the dicationic peak observed at *m*/*z* 1556.1 corresponding to $[\{(p\text{-cymene})_2Ru_2(OO\cap OO)(UPy)_2\}_2 + 2CF_3SO_3]^{2+}$. The full MS spectrum and an expansion on the relevant peaks are given in Fig. ESI8 and ESI9.†

Acknowledgements

This work was supported by the University of Neuchâtel, the Neuchâtel Platform of Analytical Chemistry (NPAC), and the Swiss National Science Foundation (SNSF) with grant no. 200020-152716 and the Ecole Polytechnique Fédérale de Lausanne (EPFL). D. C. is thankful to Scott Sneddon for computational tests run at the University of St Andrews and to Dr Pascal Mieville and Dr Daniel Jana for assistance and help in establishing remote access to the cluster located at the EPFL and used for the DFT calculations.

References

1 J. W. Steed, J. L. Atwood and P. A. Gale, in *Supramolecular Chemistry: From Molecules to Nanomaterials*, ed. P. A. Gale and J. W. Steed, John Wiley & Sons Ltd., Chichester, UK, 2012, vol. 1, pp. 3–7.
2 J.-M. Lehn, *Top. Curr. Chem.*, 2012, **322**, 1–32.
3 L. M. Greig, B. M. Kariuki, S. Habershon, N. Spencer, R. L. Johnston, K. D. M. Harris and D. Philp, *New J. Chem.*, 2002, **26**, 701–710.
4 Y. Hisamatsu, N. Shirai, S.-I. Ikeda and K. Odashima, *Org. Lett.*, 2009, **11**, 4342–4345.
5 Y. Yang, M. Xue, L. J. Marshall and J. de Mendoza, *Org. Lett.*, 2011, **13**, 3186–3189.
6 B. Gong, *Acc. Chem. Res.*, 2012, **45**, 2077–2087.
7 W. P. J. Appel, M. M. L. Nieuwenhuizen, M. Lutz, B. F. M. de Waal, A. R. A. Palmansa and E. W. Meijer, *Chem. Sci.*, 2014, **5**, 3735–3745.
8 L. Brunsveld, B. J. B. Folmer, E. W. Meijer and R. P. Sijbesma, *Chem. Rev.*, 2001, **101**, 4071–4097.
9 O. A. Scherman, G. B. W. L. Ligthart, H. Ohkawa, R. P. Sijbesma and E. W. Meijer, *Proc. Natl. Acad. Sci. U. S. A.*, 2006, **103**, 11850–11855.
10 R. P. Sijbesma, F. H. Beijer, L. Brunsveld, B. J. B. Folmer, J. J. K. K. Hirschberg, R. F. M. Lange, J. K. L. Lowe and E. W. Meijer, *Science*, 1997, **278**, 1601–1604.
11 S. H. M. Söntjens, R. P. Sijbesma, M. H. P. van Genderen and E. W. Meijer, *J. Am. Chem. Soc.*, 2000, **122**, 7487–7493.
12 G. D. Lei, Y. Yi, Z. Y. Lu and M. G. Xie, *Chin. Chem. Lett.*, 2005, **16**, 1185–1188.
13 N. Roy, E. Buhler and J.-M. Lehn, *Chem. – Eur. J.*, 2013, **19**, 8814–8820.
14 S. V. Kolotuchin and S. C. Zimmerman, *J. Am. Chem. Soc.*, 1998, **120**, 9092–9093.
15 P. S. Corbin and S. C. Zimmerman, *J. Am. Chem. Soc.*, 1998, **120**, 9710–9711.
16 F. H. Beijer, H. Kooijman, A. L. Spek, R. P. Sijbesma and E. W. Meijer, *Angew. Chem., Int. Ed.*, 1998, **37**, 75–78.
17 L. Sánchez, M. T. Rispens and J. C. Hummelen, *Angew. Chem., Int. Ed.*, 2002, **41**, 838–840.
18 X.-Q. Li, D.-J. Feng, X.-K. Jiang and Z.-T. Li, *Tetrahedron*, 2004, **60**, 8275–8284.
19 F. H. Beijer, R. P. Sijbesma, H. Kooijman, A. L. Spek and E. W. Meijer, *J. Am. Chem. Soc.*, 1998, **120**, 6761–6769.
20 L. J. Marshall and J. de Mendoza, *Org. Lett.*, 2013, **15**, 1548–1551.
21 B. Therrien, *CrystEngComm*, 2015, **17**, 484–491.
22 T. R. Cook and P. J. Stang, *Chem. Rev.*, 2015, **115**, 7001–7045.

23 B. Therrien, G. Süss-Fink, P. Govindaswamy, A. K. Renfrew and P. J. Dyson, *Angew. Chem., Int. Ed.*, 2008, **47**, 3773–3776.

24 F. Schmitt, J. Freudenreich, N. P. E. Barry, L. Juillerat-Jeanneret, G. Süss-Fink and B. Therrien, *J. Am. Chem. Soc.*, 2012, **134**, 754–757.

25 M. A. Furrer, J. Furrer and B. Therrien, *Organometallics*, 2012, **31**, 3149–3154.

26 J. Freudenreich, C. Dalvit, G. Süss-Fink and B. Therrien, *Organometallics*, 2013, **32**, 3018–3033.

27 T. D. W. Claridge, *High-resolution NMR techniques in organic chemistry*, Elsevier, Oxford, 2nd edn, 2009.

28 D. Neuhaus and M. P. Williamson, *The nuclear Overhauser effect in structural and conformational analysis*, Wiley, New York, 2nd edn, 2000.

29 A. A. Bothner-By, R. L. Stephens, J.-M. Lee, C. D. Warren and R. W. Jeanloz, *J. Am. Chem. Soc.*, 1984, **106**, 811–813.

30 A. Bax and D. G. Davis, *J. Magn. Reson.*, 1985, **63**, 207–213.

31 R. G. Parr and W. Yang, *Density-Functional Theory of Atoms and Molecules*, Oxford Univ. Press, Oxford, 1989.

32 A. Bagno, F. Rastrelli and G. Saielli, *J. Phys. Chem. A*, 2003, **107**, 9964–9973.

33 C. Bonhomme, C. Gervais, F. Babonneau, C. Coelho, F. Pourpoint, T. Azaïs, S. E. Ashbrook, J. M. Griffin, J. R. Yates, F. Mauri and C. J. Pickard, *Chem. Rev.*, 2012, **112**, 5733–5779.

34 D. Carnevale, P. Wormald, B. Ameduri, R. Tayouo and S. E. Ashbrook, *Macromolecules*, 2009, **42**, 5652–5659.

35 D. Carnevale, V. del Amo, D. Philp and S. E. Ashbrook, *Tetrahedron*, 2010, **66**, 6238–6250.

36 M. Castro, V. R. Seymour, D. Carnevale, J. M. Griffin, S. E. Ashbrook, P. A. Wright, D. C. Apperley, J. E. Parker, S. P. Thompson, A. Fecant and N. Bats, *J. Phys. Chem. C*, 2010, **114**, 12698–12710.

37 N. Salvi, J. Frey, D. Carnevale, M. Grätzel and G. Bodenhausen, *Dalton Trans.*, 2014, **43**, 6389–6395.

38 D. Carnevale, A. J. Perez Linde, G. Bauer and G. Bodenhausen, *Chem. Phys. Lett.*, 2013, **580**, 172–178.

39 D. Carnevale, S. E. Ashbrook and G. Bodenhausen, *RSC Adv.*, 2014, **4**, 56248–56258.

40 M. W. Stanford, F. R. Knight, K. S. Athukorala Arachchige, P. S. Camacho, S. E. Ashbrook, M. Bühl, A. M. Z. Slawin and J. D. Woollins, *Dalton Trans.*, 2014, **43**, 6548–6560.

41 F. R. Knight, R. A. M. Randall, K. S. Athukorala Arachchige, L. Wakefield, J. M. Griffin, S. E. Ashbrook, M. Bühl, A. M. Z. Slawin and J. D. Woollins, *Inorg. Chem.*, 2012, **51**, 11087–11097.

42 A. M. Jones, T. Lebl, S. Patterson, T. van Mourik, H. A. Früchtl, D. Philp, A. M. Z. Slawin and N. J. Westwood, *Tetrahedron*, 2009, **65**, 563–578.

43 S. J. F. Vincent, C. Zwahlen, C. B. Post, J. W. Burgner and G. Bodenhausen, *Proc. Natl. Acad. Sci. U. S. A.*, 1997, **94**, 4383–4388.

44 MOPAC2012, J.J.P. Stewart, Stewart Computational Chemistry, Version 13.073W web: http://OpenMOPAC.net.

45 A. Garci, S. Marti, S. Schürch and B. Therrien, *RSC Adv.*, 2014, **4**, 8597–8604.

46 A. J. Cohen, P. Mori-Sanchez and W. Yang, *Science*, 2008, **321**, 792.

47 Y. Zhao and D. G. Truhlar, *J. Phys. Chem. A*, 2006, **110**, 13126.

48 Y. Zhao and D. G. Truhlar, *Theor. Chem. Acc.*, 2008, **120**, 215.

49 A. D. Becke, *J. Chem. Phys.*, 1993, **98**, 5648.

50 C. Lee, W. Yang and R. G. Parr, *Phys. Rev. B: Condens. Matter*, 1988, **37**, 785.

51 M. J. Frisch, G. W. Trucks, H. B. Schlegel, G. E. Scuseria, M. A. Robb, J. R. Cheeseman, G. Scalmani, V. Barone, B. Mennucci, G. A. Petersson, H. Nakatsuji, M. Caricato, X. Li, H. P. Hratchian, A. F. Izmaylov, J. Bloino, G. Zheng, J. L. Sonnenberg, M. Hada, M. Ehara, K. Toyota, R. Fukuda, J. Hasegawa, M. Ishida, T. Nakajima, Y. Honda, O. Kitao, H. Nakai, T. Vreven, J. A. Montgomery Jr., J. E. Peralta, F. Ogliaro, M. Bearpark, J. J. Heyd, E. Brothers, K. N. Kudin, V. N. Staroverov, R. Kobayashi, J. Normand, K. Raghavachari, A. Rendell, J. C. Burant, S. S. Iyengar, J. Tomasi, M. Cossi, N. Rega, J. M. Millam, M. Klene, J. E. Knox, J. B. Cross, V. Bakken, C. Adamo, J. Jaramillo, R. Gomperts, R. E. Stratmann, O. Yazyev, A. J. Austin, R. Cammi, C. Pomelli, J. W. Ochterski, R. L. Martin, K. Morokuma, V. G. Zakrzewski, G. A. Voth, P. Salvador, J. J. Dannenberg, S. Dapprich, A. D. Daniels, Ö. Farkas, J. B. Foresman, J. V. Ortiz, J. Cioslowski and D. J. Fox, *Gaussian 09, Revision A.01*, Gaussian, Inc., Wallingford CT, 2009.

52 P. J. Hay and W. R. Wadt, *J. Chem. Phys.*, 1985, **82**, 270.

53 W. R. Wadt and P. J. Hay, *J. Chem. Phys.*, 1985, **82**, 284.

54 P. J. Hay and W. R. Wadt, *J. Chem. Phys.*, 1985, **82**, 299.

55 J. Tomasi, B. Mennucci and R. Cammi, *Chem. Rev.*, 2005, **105**, 2999.

56 D. Zeroka and H. F. Hameka, *J. Chem. Phys.*, 1966, **45**, 300.

57 R. Ditchfield, *J. Chem. Phys.*, 1972, **56**, 5688.